Excited-state non-radiative decay in stilbenoid compounds

Izquierdo, Maria A.; Shi, Junqing; Oh, Sangyoon; Park, Soo Young; Milian-Medina, Begona; Gierschner, Johannes; Roca-Sanjuan, Daniel

Published in:
Physical Chemistry Chemical Physics

DOI:
10.1039/c9cp03308d

Publication date:
2019

PCCP

PAPER

View Article Online
View Journal | View Issue

Cite this: *Phys. Chem. Chem. Phys.*, 2019, **21**, 22429

Excited-state non-radiative decay in stilbenoid compounds: an *ab initio* quantum-chemistry study on size and substituent effects†

María A. Izquierdo,[ab] Junqing Shi,[cf] Sangyoon Oh,[d] Soo Young Park,[d] Begoña Milián-Medina,[ce] Johannes Gierschner[c] and Daniel Roca-Sanjuán*[b]

In the framework of optoelectronic luminescent materials, non-radiative decay mechanisms are relevant to interpret efficiency losses. These radiationless processes are herein studied theoretically for a series of stilbenoid derivatives, including distyrylbenzene (DSB) and cyano-substituted distyrylbenzene (DCS) molecules *in vacuo*. Given the difficulties of excited-state reaction path determinations, a simplified computational strategy is defined based on the exploration of the potential energy surfaces (PES) along the elongation, twisting, and pyramidalization of the vinyl bonds. For such exploration, density functional theory (DFT), time-dependent (TD)DFT, and complete-active-space self-consistent field/complete-active-space second-order perturbation theory (CASSCF/CASPT2) are combined. The strategy is firstly benchmarked for ethene, styrene, and stilbene; next it is applied to DSB and representative DCS molecules. Two energy descriptors are derived from the approximated PES, the Franck–Condon energy and the energy gap at the elongated, twisted, and pyramidalized structures. These energy descriptors correlate fairly well with the non-radiative decay rates, which validates our computational strategy. Ultimately, this strategy may be applied to predict the luminescence behavior in related compounds.

Received 11th June 2019,
Accepted 25th September 2019

DOI: 10.1039/c9cp03308d

rsc.li/pccp

1. Introduction

Light-emitting π-conjugated organic materials are being increasingly used for technology applications such as sensors, photoswitches, bioprobes, and light emitting diodes, among others.[1–3] Currently, one of the challenges for further progress in the field is to get a deep understanding of the structure–property relationships, and these are not easy to establish.[4] For instance, within the class of luminescent organic solids, it is well-known that some compounds are non-luminescent in solution and become bright in the solid state, but this behavior can be modified by introducing some substitution patterns in the molecules, as shown by Oelkrug *et al.* for distyrylbenzene (DSB) derivatives.[5–7] To this class of DSB derivatives belongs the distyrylbenzene cyano substituted (DSC) family of compounds (Fig. S1, ESI†), comprising all possible combinations of non-/emissive in solution/solid state phases.[5,7–10] Clearly the luminescence properties of the DSB derivatives are influenced by intra- and inter-molecular factors.[11,12] These factors have been disentangled for DCS compounds through a combined experimental and quantum chemical study.[13] A cornerstone of this work has been the explanation of the solid state luminescence enhancement (SLE) of practically non-luminescent molecules in solution.

Understanding or even predicting non-radiative deactivation processes in fluid solution is highly relevant for SLE applications in materials science as well as for designing fluorescent dyes in analytical or life sciences.[14,15] Traditionally, non-/radiative processes have been understood in terms of the Fermi's Golden rule (FGR), relying on the vibrational wavefunction overlap between the initial (i) and final (f) electronic states. This approach leads to the so-called 'energy gap law', which predicts an increase of the non-radiative decay rate (k_{nr}) with a decrease

[a] *Zernike Institute for Advanced Materials, University of Groningen, Nijenborgh 4, 9747 AG Groningen, The Netherlands*
[b] *Institute of Molecular Science, University of Valencia, P.O. Box 22085, ES-46071 Valencia, Spain. E-mail: daniel.roca@uv.es*
[c] *Madrid Institute for Advanced Studies, IMDEA Nanoscience, Calle Faraday 9, Campus Cantoblanco, 28049 Madrid, Spain*
[d] *Center for Supramolecular Optoelectronic Materials and WCU Hybrid Materials Program, Department of Materials Science and Engineering, Seoul National University, ENG 445, Seoul 151-744, Korea*
[e] *Department for Physical Chemistry, Faculty of Chemistry, University of Valencia, Av. Dr Moliner 50, 46100 Burjassot, Spain*
[f] *Xi'an Institute of Flexible Electronics, Northwestern Polytechnical University, Dongda Town, Dongxiang Street 1, 710072 Xi'an, Shaanxi, China*

† Electronic supplementary information (ESI) available: Chemical structures of the DCS family; active orbitals used for the CASSCF/CASPT2 computations. See DOI: 10.1039/c9cp03308d

of the energy gap between the ground (S_0) and excited (S_1) states. Such approach may be applicable to rigid molecular structures, due to small geometrical displacements between the equilibrium structures of i and f.[14] However, FGR-based approaches may fail for flexible molecules where the topology of S_0 and S_1 differ significantly and where the non-radiative decay process is driven by a conical intersection (CI).[15–27] CI-based mechanisms have also been highlighted for rigid polyaromatic hydrocarbons (PAHs).[20]

Multiconfigurational methods with dynamic electron correlation, such as the complete-active-space self-consistent field/complete-active-space second-order perturbation theory (CASSCF/CASPT2), are suitable to describe CIs.[18,19,28,29] These methods are however computationally expensive, especially when large and highly π-conjugated systems involving many chemically-active orbitals are studied, not allowing in this case the determination of photophysical and photochemical reaction paths. Spin–flip time-dependent density functional theory (SF-TDDFT) has been shown in PAHs to help in the exploration of the CI region and determination of non-radiative decay routes.[20] An alternative approach, is to use multiconfigurational quantum chemistry within a simplified strategy for excited-state PES explorations and CI geometry optimizations. Such a strategy should be able to provide qualitative and semi-quantitative information on the excited-state photophysics and photochemistry. This approach would keep a full configuration interaction description among the chemically-active orbitals.

For instance, Estrada *et al.*[25] studied the PESs of optoelectronic materials, fluoren-9-ylidene malononitrile (FM) and indan-1-ylidene malononitrile (IM), in order to understand their excited state deactivation mechanisms. CASSCF and CASPT2 reaction path determinations for a model system, namely, 1,1-dicyanoethylene (DCE), were carried out. The knowledge acquired for DCE was used to derive approximated PESs for IM and FM, and to interpret the experimentally observed radiationless decay lifetimes. Similarly, El-Zohry *et al.*[26] studied the photochemistry of the indoline donor unit in attempts to understand the energy losses of indoline-based dye-sensitized solar cells. A CASPT2 exploration of the PESs revealed an ethene-like photodynamics mechanism, which is activated through a CI.[30–34] This mechanism turned out to compete with the charge separation process, as suggested by the short excited-state lifetimes.

For a set of DCS compounds, an intriguing dependence of the luminescence character with the position of the cyano groups, either α or β respect to the central benezene ring (see Fig. S1, ESI†), has been found.[13] In fluid solution, α-compounds are, generally, less emissive than β-compounds. The excitation energy at the Franck–Condon (FC) region of α compounds is higher than that of β compounds, driven by enhanced resonance stabilization (ERS) of the latter.[13] Approximate PESs, computed by TDDFT, follow a decay path towards a surface crossing region by twisting the vinyl bond of the molecule. This PES's pattern and analyses of the de-/localized character of the natural orbitals at the twisted structures (obtained from CASSCF computations), led to the following hypothesis for a given α- and β-DCS pair: the difference between the CI energy is not as large as the difference between the FC energies. If so, it would imply that the CI of α-compounds is more accessible (or less restricted) than that of β-compounds, and consequently the emissive character of the former is lower than that of latter, as suggested by the experimental data.

The above-mentioned experimental and computational study has been recently extended from representative to all available DCS compounds.[36] It has confirmed that the higher the absorption energy, the lower the experimental fluorescence quantum yields (Φ_F) due to an increase of k_{nr}. This finding is opposite to the conventional energy gap law, establishing an 'inverted energy gap law' for emissive floppy DCS materials; that is, the higher the FC energy, the higher the k_{nr}.[35]

Despite the relevant findings on the non-radiative deactivation of DCS compounds reported in the preceding studies,[13,35] several questions remain open. Most importantly, high-level exploration of the radiationless decay channels is required, focusing on a deeper and higher-accuracy study of the CI that funnels the energy from the excited to the ground state in the non-radiative decay process. This is done herein by using an *ab initio* TFDFT and CASPT2 quantum chemistry approach in order to understand the main electronic-structure properties of the CI and the non-radiative decay mechanisms. This is of particular importance as it turned out that although the increase of the k_{nr} with the FC energy is generally valid, there are exceptions to this 'inverted energy gap law'. For example, the *meta*-tetrafluoromethyl DCS pair (α,β-TFDCS), see Fig. 1, follows an 'energy gap law'. The k_{nr} of α-TFDCS is smallertthan that of β-TFDCS, with 25.1 and 85.1 ns^{-1}, respectively. However, the FC energy of α-TFDCS is higher than that of β-TFDCS, with 3.1 and 2.9 eV (TDDFT), respectively.[13,35]

In this work, similarly to the above-mentioned studies by Estrada *et al.*[25] and El-Zohry *et al.*,[26] a simplified strategy to explore PESs and decay routes is designed to study the DCS compounds. The implementation of a simplified strategy is justified by the size and electronic-structure features of the systems under study. Such a strategy is based on geometrical changes of the excited state, including three nuclear coordinates around the vinyl bond. These coordinates are the elongation, torsion, and pyramidalization of one of the ethylenic carbon atoms. Our emerging approach is firstly compared and benchmarked

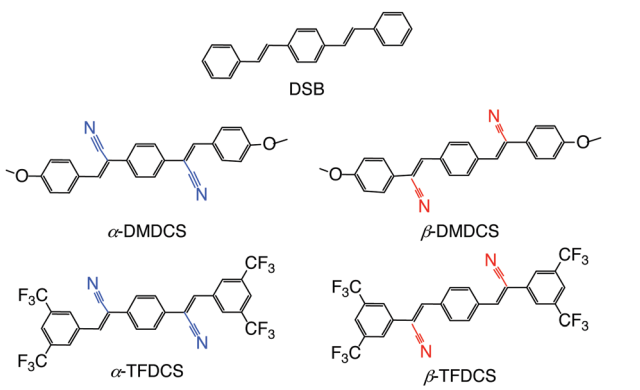

Fig. 1 Chemical structures of the DCS molecules studied in this work.

for well-known molecules, *i.e.*, ethene,[30] styrene,[31,32] and stilbene,[33,34,36] with a more accurate approach based on a fully unconstrained determination of the CI. Next, our approach is applied to the distyrylbenzene (DSB) molecule and to four representative molecules of the DCS family. The last includes representative pairs of the 'inverted energy gap law' and the 'energy gap law', namely, the *para*-di-methoxy DCS pair (α,β-DMDCS) and the *meta*-tetrafluoromethyl DCS pair (α,β-TFDCS), respectively (see Fig. 1; for DSB and the entire α,β-DCS family see Fig. S1, ESI†).

Closely related to α,β-DMDCS stands the *para*-di-butoxy DCS pair, α,β-DBDCS. The FC energy of α-DBDCS is higher than that of β-DBDCS, with 3.0 and 2.6 eV (TDDFT), respectively. The k_{nr} of α-DBDCS is higher than that of β-DBDCS, with 250 and 0.39 ns^{-1}, respectively.[13,35] No significant differences are expected for α,β-DMDCS.

Finally, simple energy descriptors are established to predict the experimental trends, the FC energy and the energy gap at the near-degeneracy region.

2. Computational details

DFT, TDDFT, and CASSCF/CASPT2[19,28,29] methods were used to study the radiationless decay mechanisms of ethene, styrene, stilbene, α,β-DMDCS, and α,β-TFDCS. S_0 and S_1 geometry optimizations of minima were carried out by using DFT and TDDFT, respectively. The CAM-B3LYP exchange–correlation (XC) functional,[37] as implemented in the GAUSSIAN 09 computational software,[38] and the correlation consistent valence triple-ζ plus polarization (cc-pVTZ) basis set[39] were used.

For ethene, styrene, and stilbene, multiconfigurational methods with and without dynamic correlation were used to optimize the S_0 and S_1 minima and to determine the S_0/S_1 minimum energy conical intersections (MECIs). CASSCF and CASPT2 methods, as implemented in the MOLCAS electronic structure package,[40] together with the atomic natural orbital small-type valence double-ζ plus polarization (ANO-S-VDZP) basis set[41] were used. An active space of 2 active electrons distributed in 2 active orbitals, corresponding to the π and π* orbitals of the vinyl bond, was selected (hereafter, CASSCF(2,2) and CASPT2(2,2)), see ESI.† These orbitals are the most relevant for the characterization of the radiationless decay mechanism. No point-group symmetry constraints were used in the geometry optimization to allow all possible structural distortions.

TDDFT and CASPT2 were employed to calculate the FC energies. S_0 and S_1 PESs for the non-radiative decay paths were computed with the CASPT2 method. At the TDDFT level, the CAM-B3LYP XC functional and the cc-pVTZ basis set with/without the polarizable continuum model (PCM) for computing the $CHCl_3$ solvent implicit effects[42] were used. At the CASPT2 level, several active spaces together with the ANO-S-VDZP basis set were considered. For ethene, styrene, and stilbene, the CASPT2(2,2), CASPT2(8,8), and CASPT2(14,14) methodological approaches were used, respectively (see natural orbitals in Fig. S2–S4, ESI†). CASPT2(4,4) and CASPT2(12,12) were employed for DSB, α,β-DMDCS, and α,β-TFDCS (see natural orbitals in Fig. S5–S9, ESI†). For CASPT2 computations, an imaginary shift of 0.20 a.u. was included in order to minimize the effect of intruder states.[43] Both the conventional and ionization potential/electron affinity (IPEA)-corrected CASPT2 methods with values of 0.00 and 0.25 a.u., respectively, were considered.[44]

3. Results and discussion

3.1. Ethene, styrene, and stilbene

These ethene-like molecules are relatively small-size models that allow an accurate characterization of the radiationless decay mechanism by determining the S_0 and S_1 equilibrium structures and the S_0/S_1 CI. Geometrical and electronic structure analyses of the optimized geometries are then useful for defining an approximated strategy to study larger-size systems, such as the DCS compounds.

3.1.1. Geometrical analysis and electronic structure properties of the excited vinyl bond. The main non-radiative decay paths in ethene,[30] styrene,[31,32] and stilbene[33,34,45] have been studied in previous works, obtaining accurate details of the mechanism. Three main types of internal coordinates represent the geometrical changes taking place along S_1 PES, from the FC region to the S_0/S_1 CI that funnels the population of S_1 to S_0 without light emission. These coordinates correspond to the vinyl bond length, d_{CC}, the rotational dihedral angle, ϕ, and the pyramidalization or inversion angle, τ, which are displayed in Fig. 2.

Hence, the geometry of ethene-like molecules at the CI possesses an elongated, twisted, and pyramidalized vinyl bond. In this work, geometry optimizations of S_0 and S_1 minima and the S_0/S_1 MECIs of ethene,‡ styrene, and stilbene were computed at the CASSCF(2,2) and CASPT2(2,2) levels (where only the π orbitals of the vinyl bond are included in the active space). The obtained values for d_{CC}, ϕ, and τ are compiled in Table 1, which also lists the geometrical parameters, when available, as reported in the literature. The MECIs of ethene, styrene, and stilbene obtained in this work are displayed in Fig. 3.

For ethene, styrene, and stilbene, the MECI geometries obtained with CASSCF(2,2) or CASPT2(2,2) are comparable to those obtained with more accurate multiconfigurational methodologies, with larger active spaces, as those reported in the literature.[30,31,33] Such results indicate that the use of reduced active spaces is reasonable for locating the geometry of the CI in large molecules.

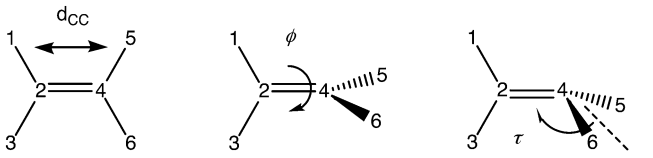

Fig. 2 Main geometrical parameters that characterize the S_0/S_1 CI of the ethene-like molecules studied in this work, vinyl bond length, d_{CC}, the rotational dihedral angle, ϕ, and the pyramidalization or inversion angle, τ.

‡ The S_1 geometry is not a real minimum but a consequence of the computation starting by a planar structure. Nevertheless, it illustrates the geometrical changes in the radiationless decay path.

Table 1 CASSCF(2,2) and CASPT2(2,2) geometrical parameters of the optimized S_0 and S_1 minima and the S_0/S_1 CI of ethene-like molecules: vinyl bond length, d_{CC} (in Å), the rotational dihedral angle, ϕ (in °), and the pyramidalization or inversion angle, τ (in °)

		d_{CC}	ϕ	τ	d_{CC}	ϕ	τ	d_{CC}	τ
Molecule	State	CASSCF(2,2)			CASPT2(2,2)			Reported[a]	
Ethene	S_0-min	1.33	180.0	180.0	1.36	180.0	180.0	1.34	180.0
	S_1-min	1.44	180.0	180.0	1.49	180.0	180.0		
	S_0/S_1 CI	1.39	113.3[b]	105.0	1.42	108.5[b]	104.0	1.45	103.0
Styrene	S_0-min	1.33	180.0	180.0	1.36	180.0	180.0	1.37	180.0
	S_1-min	1.41	180.0	180.0	1.40	180.0	179.0		
	S_0/S_1 CI	1.40	116.1[b]	114.0	1.43	116.1[b]	111.0	1.42	104.1
Stilbene	S_0-min	1.33	180.0	180.0	1.37	180.0	180.0	1.37	180.0
	S_1-min	1.41	180.0	178.2	1.43	180.0	180.0		
	S_0/S_1 CI	1.40	119.7[b]	110.9	1.47	110.5[b]	100.2	1.39	101.0

[a] Reported values for ethene,[30] styrene,[31] and stilbene[45] correspond to CASPT2(2,2), CASPT2(12,12) and CASPT2(14,14), respectively. [b] Due to the asymmetry in the pyramidalization, two angles are possible, showing here only the smallest one.

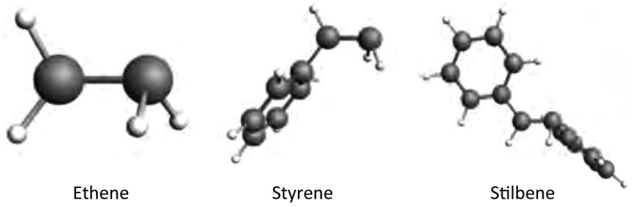

Fig. 3 MECI geometries of ethene, styrene, and stilbene. See CASSCF(2,2) and CASPT2(2,2) main geometrical parameters in Table 1.

The deformation of the vinyl bond upon radiation can be interpreted in terms of the electronic structure. Fig. 4 shows a scheme with the main features of the electronic structure of S_0 and S_1 at the FC and CI regions. The excited state at the FC region is characterized by the population of the π^* orbital, which weakens the vinyl bond and permits rotation around it with no energy barrier or small activation energy. At the CI region, the degenerate electronic states are mainly characterized by two electronic configurations, a biradical configuration, with one electron at each carbon atom, and a zwitterionic or ionic configuration, with two electrons in the pyramidalized carbon atom.[31,45]

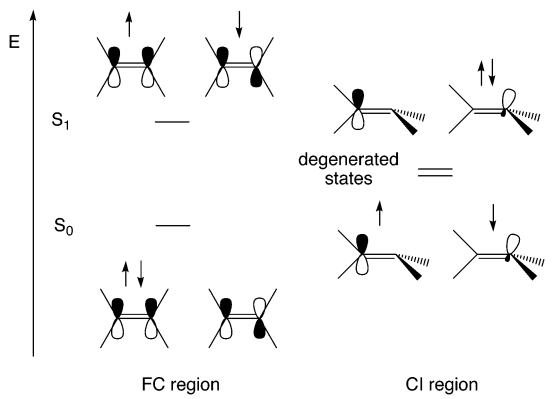

Fig. 4 Molecular orbital diagram for ethene-like molecules at the FC and S_0/S_1 CI regions.

3.1.2. Computational strategy to explore the non-radiative decay paths. Being aware that the study of radiationless mechanisms of the DCS molecules is quite challenging, both theoretically and computationally, we searched for an affordable and reasonable computational strategy to approximate S_0/S_1 CIs. A potential strategy would consist of the characterization of the S_0 and S_1 PESs, between the FC and CI regions, as a function of the vinyl bond elongation and the coupled torsion and pyramidalization coordinates, indicated in Fig. 2.

A similar modelling procedure has been already applied to styrene as well as to malononitrile and indoline derivatives.[25,26,31] The symmetry properties of these molecules at the twisted vinyl bond have been used to optimize the geometry of the zwitterionic state and to explore the CI region (see more details in ref. 25). Unfortunately, the DCS compounds lack symmetry properties at the twisted geometry and at the CI. S_0 and S_1 PES scans including geometry optimizations, *via* multiconfigurational methods, would be very costly and would not ensure the connectivity between converged points. Alternatively, one might take benefit of DFT and TDDFT for geometry optimizations and use a high-level method such as CASPT2 for the energy profiles. Thus, our strategy is defined as follows: (1) DFT optimization of the ground-state equilibrium geometry, S_0-min, (2) TDDFT optimization of the excited-state equilibrium geometry giving in general a planar structure, S_1-min, (3) TDDFT optimization of S_1 at the twisted geometry, S_1-bend (where the dihedral angle is constrained to 90°, as shown in Fig. 2, and the remaining internal coordinates are allowed to relax), (4) linear interpolation of internal coordinates (LIICs) between the previous structures, (5) pyramidalization of one of the carbon atoms of the vinyl bond (and its connected groups) from S_1-bend,[46] by varying τ from 180° up to 90° in steps of 10° maintaining all the other internal coordinates fixed, and (6) CASSCF/CASPT2 energies for the geometries generated in 4 and 5.

As an illustrative example of the internal coordinates that involves this approach, Fig. 5 shows the geometry evolution from S_0-min to the approximate CI structure of ethene, which is reached upon pyramidalization.

The above-mentioned computational strategy was applied to ethene, styrene, and stilbene. The results obtained together with the energy position of the optimized MECI (red dash line) are displayed in Fig. 6. For completeness, Fig. 7 displays the approximated conical intersections (ACIs) of ethene, styrene, and stilbene. It can be seen that the main features of the non-radiative mechanism are captured with our approximated strategy. The energy gap between the S_0 and S_1 PESs reduces

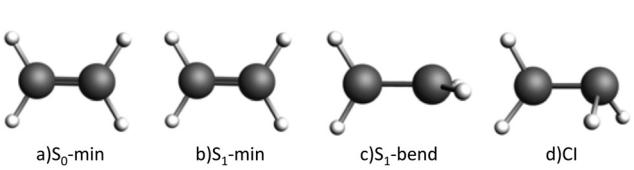

Fig. 5 Main geometries that characterize the non-radiative decay mechanism of ethene and define our computational strategy to determine such a mechanism in DCS molecules, (a) ground-state equilibrium geometry, (b) planar excited-state equilibrium geometry, (c) excited-state twisted optimized geometry and (d) approximated CI.

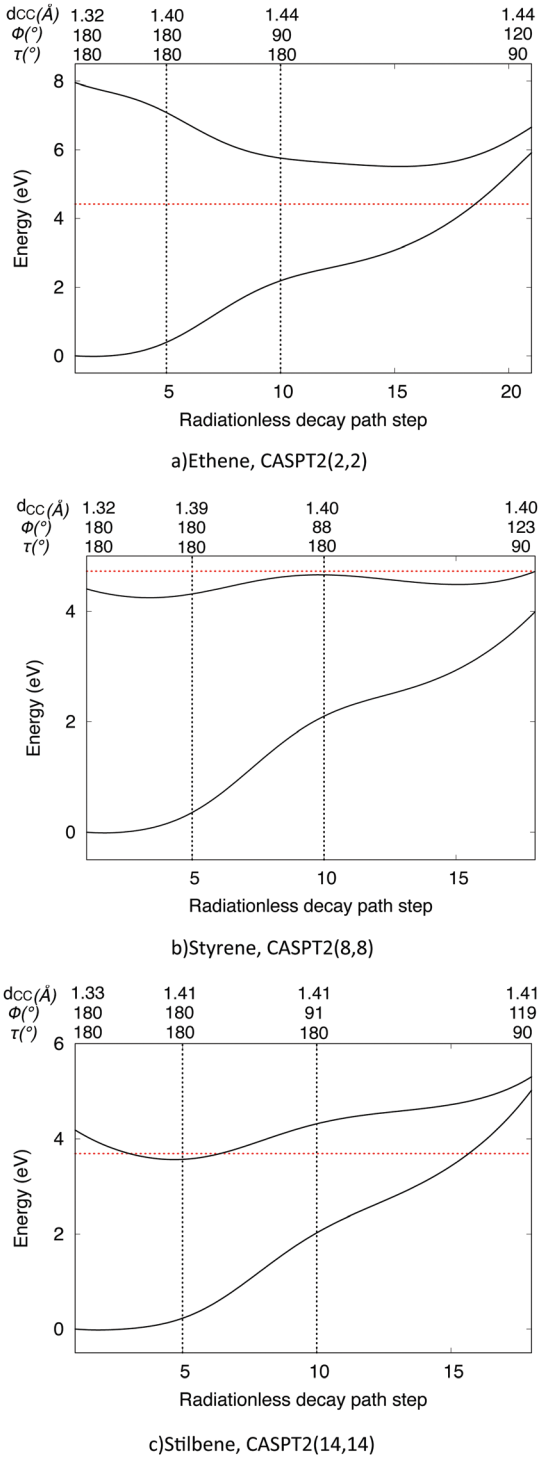

Fig. 6 Approximate CASPT2 S_0 and S_1 PESs of ethene (a), styrene (b), and stilbene (c) as function of the coupled elongation, torsion, and pyramidalization coordinates. From step 1 to 5 (Elongation), LIICs between S_0-min and S_1-min; from step 6 to 9 (Torsion), LIICs between S_1-min and S_1-bend; from step 10 to 18 (Pyramidalization), pyramidalization of the CH_2 group of the vinyl bond in ethene and styrene and the $-CHC_5H_5$ part in stilbene, with τ intervals of 10°. The red dash line represents the MECI relative to that of the S_0-min computed at the same level of theory as for the paths (black curves). Smooth Bézier[49] curves are shown for the sake of clarity.

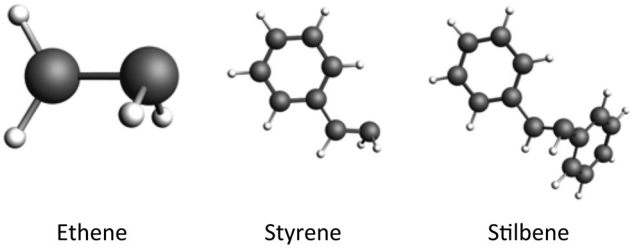

Fig. 7 ACI geometries of ethene, styrene, and stilbene.

upon elongation, torsion, and pyramidalization. While for ethene no well is found in the elongation part, it does appear for styrene and stilbene. Such minima are responsible for the fluorescence yield reported for those compounds (around 0.25[47] and 0.05,[48] respectively). Note that the lower yield of stilbene can be attributed to the relative position of the MECI. The energy of this crossing appears below the S_1 energy at the FC region and slightly above that of S_1-min (step 5 of the radiationless decay path). For styrene, with a higher yield, the MECI appears slightly above the S_0 and S_1 profiles. As compared to the MECI, the employed strategy overestimates the crossings, particularly for stilbene. Then, these approximated CI energies cannot be used as quantities to predict the accessibility to the crossing. These should be used instead as entities to qualitatively estimate the photophysics of the molecules under study.

3.2. DSB, α-DMDCS, β-DMDCS, α-TFDCS, and β-TFDCS

The above-discussed computational strategy appears to be qualitatively good for rationalizing the main features of the radiationless mechanism of ethene-like molecules, overestimating the CI. In this section, our strategy is used to explore the non-radiative decays of the DSB molecule and four representative compounds of the DCS family, namely α-DMDCS, β-DMDCS, α-TFDCS, and β-TFDCS (see Fig. 1). The aim is to derive (computationally efficient) descriptors that support the luminescence properties of the DCS molecules in question. As described in the introduction, while k_{nr} for the *para*-alkoxy substituted compounds is much larger in α-isomer (250 ns^{-1}) than in the β one (0.39 ns^{-1}), the opposite trend is found for α-TFDCS (25.1 ns^{-1}) and β-TFDCS (85.1 ns^{-1}). We also attempt to generalize the factors that rule the luminescence properties across the DCS family and related systems. Properties across the DCS family and related systems.

3.2.1. Absorption, emission, and adiabatic energies. The vertical absorption energy (E_{va}) is defined as the energy difference between S_0 and S_1 states, both at the optimized S_0 geometry. The vertical emission energy (E_{ve}) is defined as the energy difference between S_0 and S_1 states, both at the optimized S_1 geometry. The adiabatic energy (E_{ad}) is defined as the energy difference between S_0 and S_1 states, at the optimized S_0 and S_1 geometries, respectively. E_{va}, E_{ve} and E_{ad} obtained with several theoretical methodologies are herein compared to the experimental data. The comparisons will allow us to evaluate the relative accuracy of (1) the XC functional (hybrid or long-range corrected (LC)), (2) the basis sets, and (3) the active space and IPEA shift of the

Table 2 Vertical absorption energy (E_{va}), vertical emission energy (E_{ve}), and adiabatic energy (E_{ad}) (in eV) of α-DMDCS and β-DMDCS computed at distinct levels of theory and corresponding experimental data

	α-DMDCS			β-DMDCS		
Methodology[a]	E_{va}	E_{ve}	E_{ad}	E_{va}	E_{ve}	E_{ad}
B3LYP/6-311G*/PCM[b]	3.04	2.41	2.62	2.61	2.17	2.46
CAM-B3LYP/cc-pVTZ	3.60	2.84	3.20	3.20	2.69	2.96
CAM-B3LYP/cc-pVTZ/PCM	3.49	2.70	3.05	3.06	2.44	2.78
CASPT2(4,4)/ANO-S-VDZP	3.15	2.56	2.57	2.94	2.42	2.41
CASPT2(12,12)/ANO-S-VDZP	3.26	2.69	2.80	2.92	2.44	2.42
CASPT2(4,4)/ANO-S-VDZP/IPEA	3.90	3.27	3.31	3.69	3.13	3.17
CASPT2(12,12)/ANO-S-VDZP/IPEA	3.92	3.21	3.36	3.53	2.94	2.97
Exp.[b]	3.45	2.70	3.00	3.30	2.50	2.85

[a] Geometry optimizations were computed with the CAM-B3LYP XC functional and the cc-pVTZ basis set, except for B3LYP/6-311G*/PCM($CHCl_3$) for which geometry optimizations were computed with the B3LYP XC functional, the 6-311G* basis set and using the PCM($CHCl_3$) model.[13] [b] Data for the equivalent α,β-dibutoxy-substituted compounds.[13]

CASPT2 method, and to estimate the solvent effects. The DFT-based approaches are B3LYP/6-311G*/PCM($CHCl_3$), CAM-B3LYP/cc-pVTZ, and CAM-B3LYP/cc-pVTZ/PCM($CHCl_3$). The CASPT2 methodologies are CASPT2(4,4), consisting of 4π electrons distributed in 4 orbitals (including 2π and 2π* orbitals mainly centered in the vinyl bonds), and CASPT2(12,12), consisting of 12π electrons distributed in 12 orbitals (including 6π and 6π* orbitals delocalized over the whole π-conjugated system). The conventional CASPT2 is compared with the IPEA-corrected CASPT2 with a value of 0.25 a.u. The corresponding E_{va}, E_{ve}, and E_{ad} values are given in Table 2.

Overall, both TDDFT and CASPT2 methodologies lead to S_0 and S_1 minima in reasonable agreement with experiments, with higher absorption energies for α-DMDCS than those for β-DMDCS. Within TDDFT methodologies, the CAM-B3LYP XC functional leads to energies closer to the experimental data. Nevertheless, the simpler B3LYP XC functional (and less costly approach) gives rise to the same relative energy trend. The inclusion of solvent, as done in the PCM, shifts only slightly the absorption and emission energies, keeping the same relative trend for α and β compounds. Within CASPT2 methodologies, CASPT2(4,4) and CASPT2(12,12) maintain the experimental trends. E_{ad} shows the largest underestimations, which is due to the fact that distinct levels of theory were used for geometry optimizations (DFT and TDDFT) and energies (CASPT2); the CASPT2 minima are slighly displaced with respect to the (TD)DFT ones. CASPT2(4,4) and CASPT2(12,12) energy differences are small, in general below 0.2 eV. When the IPEA shift is considered, the CASPT2 energies significantly deviate from the experimental data. It suggests that for these systems the IPEA shift, which is supposed to correct the description of open-shell electronic states,[44] is not adequate. Therefore, in the following, only CASPT2 energies (without the IPEA shift) are reported.

3.2.2. Systematic exploration of non-radiative decay paths of DSB, α-DMDCS, and β-DMDCS. Fig. 8 shows the S_0 and S_1 energy profiles along the radiationless decay path of DSB, α-DMDCS and β-DMDCS, derived from the computational strategy defined in the Section 3.1.2. For completeness, Fig. 9 displays the ACIs of DSB, α-DMDCS, and β-DMDCS.

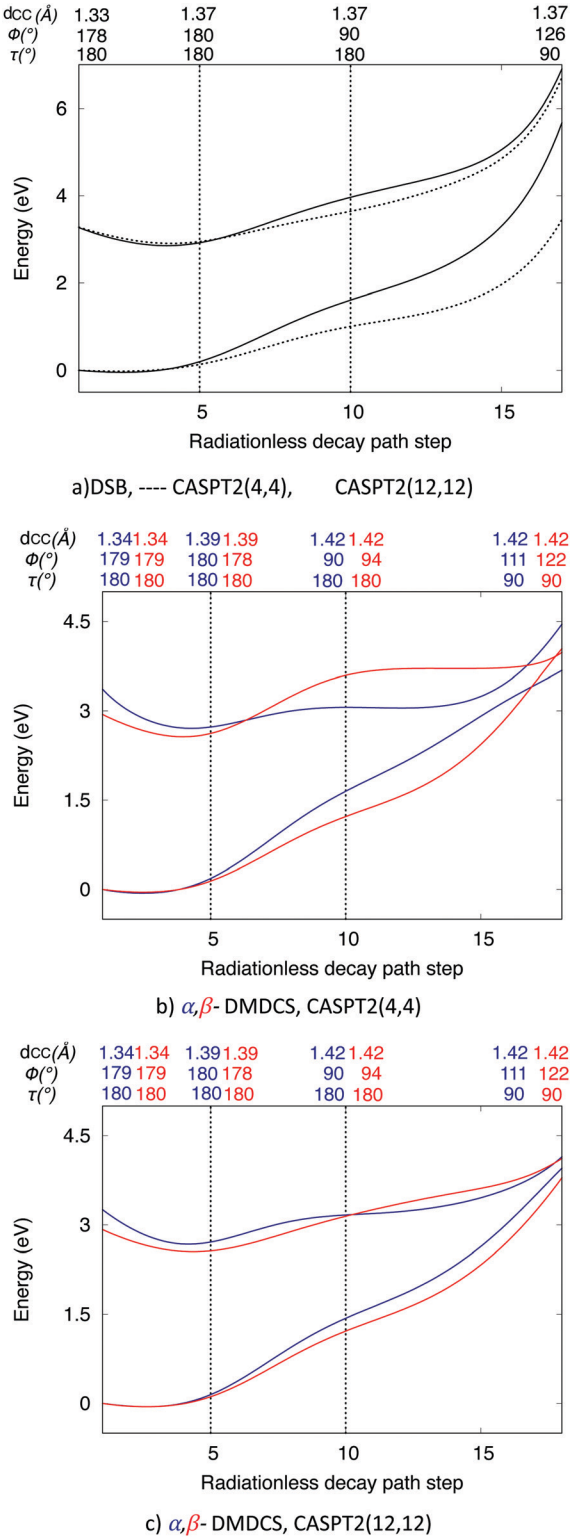

Fig. 8 Approximated CASPT2(4,4) and CASPT2(12,12) S_0 and S_1 PESs of DSB, α-DMDCS (blue curves in b and c) and β-DMDCS (red curves in b and c) as function of the coupled elongation, torsion and pyramidalization coordinates of the vinyl bond. From step 1 to 5 (Elongation), LIICs between S_0-min and S_1-min; from step 6 to 9 (Torsion), LIICs between S_1-min and S_1-bend; from step 10 to 18 (Pyramidalization), pyramidalization of the carbon atom of the vinyl bond with the cyano substituent, τ with intervals of 10°. Smooth Bézier curves are shown for the sake of clarity.

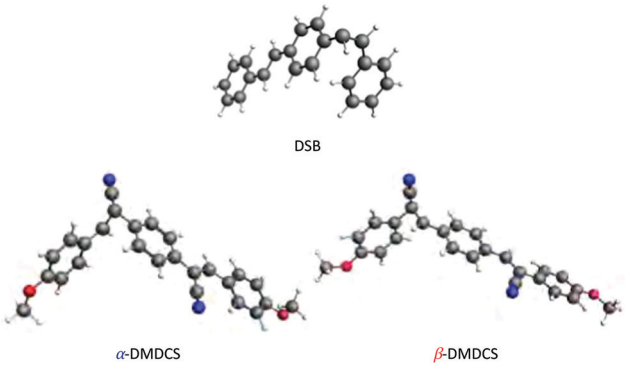

Fig. 9 ACI geometries of DSB, α-DMDCS, and β-DMDCS.

The E_{va} of DSB is 3.16 eV at the CASPT2(12,12) level. It is comparable to that of α-DMDCS and β-DMDCS but much lower than that of stilbene (Fig. 6). However, the energy gap between the S_0 and S_1 PESs do not decrease as rapidly as in the case of the DMDCS compounds in the pyramidalization region. Moreover, the narrowest S_0–S_1 energy gap of DSB appears at higher energies than that of DMDCS. These results indicate that the CI is much less accessible for DSB than for DMDCS, and consequently a radiationless decay is much less probable. This hypothesis closely fits with the highly-emissive character of DSB, which has a fluorescence quantum yield of 0.87.[8,50] Given the less accessible CI and the relatively large energy gaps in the pyramidalization region of DSB, photoisomerization in this system might take place through an adiabatic process rather than an internal conversion process, as suggested in previous studies.[51,52]

Regarding the performance of the CASPT2(4,4) and CASPT2(12,12) methodologies on the DSB energy profiles, clearly S_0 is more sensitive to the size of the CAS than S_1, especially in the pyramidalization region. In fact, at the FC region, CASPT2(4,4) and CASPT2(12,12) energies are comparable. In the pyramidalization region, CASPT2(4,4) and CASPT2(12,12) energies differ. There, the CASPT2(12,12) method is expected to be more consistent with the photophysics of DSB. Despite this, both CASPT2(4,4) and CASPT2(12,12) lead to similar qualitative pictures. For α-DMDCS and β-DMDCS, the corresponding S_0 and S_1 PESs evolve towards a region of near-degeneracy, which has the potential to activate a radiationless decay. The energy profiles are phenomenologically similar to those obtained in the previous subsection. These observations are valid for both CASPT2(4,4) and CASPT2(12,12) energy profiles. Taken together, these results support our model to determine radiationless decay channels. As already mentioned, the approximated CI must be considered only qualitatively, as its energy position relative to the S_0 energy at the FC is overestimated. Given that CASPT2(12,12) leads to more accurate results, in the following, only CASPT2(12,12) energy profiles are discussed (CASPT2(4,4) are shown by completeness only).

By comparing the S_0 and S_1 PESs of α-DMDCS and β-DMDCS, a difference in the FC region appears clear: S_1 of α-DMDCS lays at a higher energy than that of β-DMDCS. That is, the E_{va} of α-DMDCS is larger than that of β-DMDCS. It is expected that the light absorption process provides a larger kinetic energy to α-DMDCS than to β-DMDCS, for which α-DMDCS reaches much easier the CI. This reasoning agrees with the experimental evidence of a lower fluorescence yield for α than for β in alcoxy DCS isomers (the fluorescence yields of the α- and β-dibutoxy-DCS isomers are 2×10^{-3} and 0.54, respectively).§[13]

Our findings confirm a previous TDDFT study on α,β-DCS molecules free of alkoxy substituents[13] and are in agreement with a recent work in which absorption energies for the entire DCS family are computed and correlating with Φ_F and k_{nr}.[35] In the latter, E_{va}s are obtained at the B3LYP/6-311G*/PCM($CHCl_3$) level of theory, which, as shown in the Section 3.2.1, gives reasonable energies with a relatively low computational cost. Strong correlations between E_{va} and k_{nr} (or Φ_F) have been obtained pointing to a relevant role of the E_{va} to explain the luminescence properties and establishing an 'inverted gap law' for the DSC family.

Based on the results discussed in this section and those reported by Gierschner *et al.*,[13,35] the E_{va} of α compounds is, generally, higher than that of β compounds, being the main source for the more emissive properties of β compounds. These inferences may be understood in light of the discussion of the enhanced resonance stabilization (ERS), as explained by Shi *et al.*[13] The number of ionic resonance structures in the excited state with the negative charge residing on the nitrogen atoms determines the stabilization of the excited state. Such number of ionic structures is larger for β compounds than that for α compounds.

3.2.3. Systematic exploration of the non-radiative decay paths in α-TFDCS and β-TFDCS. The E_{va} seems to explain reasonably well the photophysical behavior of the α,β-DCS compounds. However, this claim fails for α-TFDCS and β-TFDCS. Both compounds are low emissive, where the E_{va} of α-TFDCS is larger than that of β-TFDCS, and the k_{nr} of α-TFDCS is smaller than that of β-TFDCS, with 25.1 and 85.1 ns^{-1}, respectively. This indicates that being restricted to the FC region leaves out some features of the photodynamics that are crucial for particular systems. Indeed, the exploration of the CI region is relevant for understanding the luminescence properties. Under this premise, the PESs of α-TFDCS and β-TFDCS, derived from our model, were explored. The corresponding energy profiles are displayed in Fig. 10. For completeness, Fig. 11 displays the ACIs of α-TFDCS, and β-TFDCS.

The main difference between α,β-DMDCS and α,β-TFDCS energy profiles appears in the pyramidalization region. The S_1 PESs of α-DMDCS and β-DMDCS switch after the torsion coordinate takes place. On the contrary, the S_1 PESs of α-TFDCS and β-TFDCS remain unswitched along the radiationless decay path. The smaller the energy gap in the pyramidalization region, the more likely the radiationless decay. Accordingly, the energy gaps at the FC and pyramidalization regions of α,β-DMDCS and α,β-TFDCS predict non-radiative decay paths for α-DMDCS and β-TFDCS, which is in agreement with the

§ The butoxy and methoxy substituents in *para* position are not expected to show significant differences for the purposes of the present analysis. Methoxy groups simplify considerably the computations.

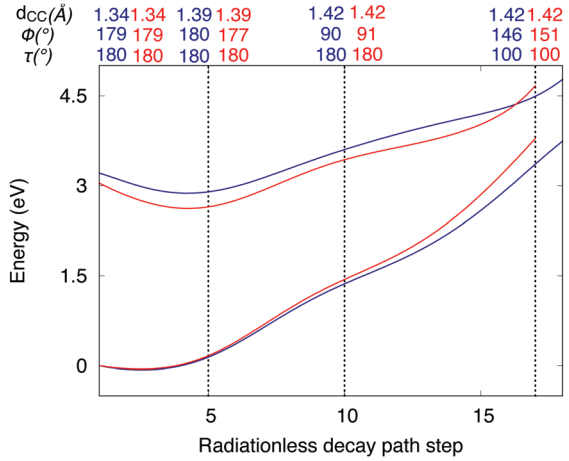

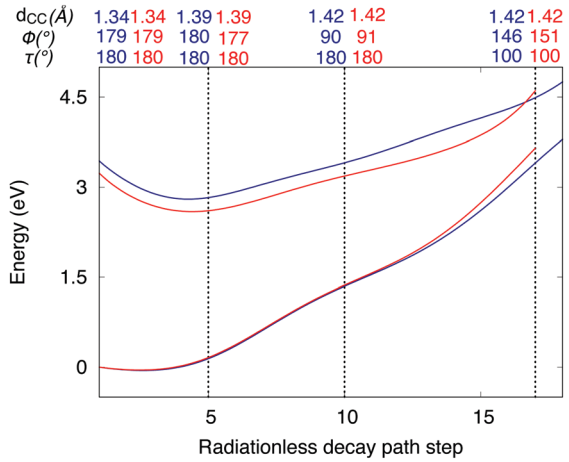

Fig. 10 Approximated CASPT2(4,4) and CASPT2(12,12) S_0 and S_1 PESs of α-TFDCS (blue curves) and β-TFDCS (red curves) as function of the coupled elongation, torsion, and pyramidalization coordinates of the vinyl bond. From step 1 to 5 (Elongation), LIICs between S_0-min and S_1-min; from step 6 to 9 (Torsion), LIICs between S_1-min and S_1-bend; from step 10 to 18 (Pyramidalization), pyramidalization of the carbon atom of the vinyl bond with the cyano substituent, τ with intervals of 10°. For β-TFDCS, the rotation τ of 90° leads to a geometry with steric effects for which it was excluded. Smooth Bézier curves are shown for the sake of clarity.

experimentally observed emissive properties and the radiationless decay rates.[35]

3.2.4. Zwitterionic stabilization. To rationalize the energy gaps at the pyramidalized structures of α,β-DMDCS and α,β-TFDCS, the electronic structure of the excited state at these geometries is analyzed, similarly as done in previous works.[25,53,54]

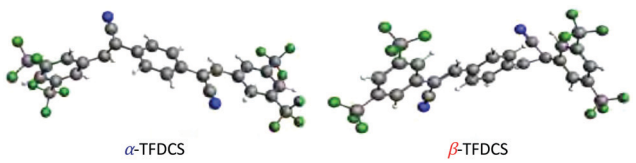

Fig. 11 ACI geometries of α-TFDCS, and β-TFDCS.

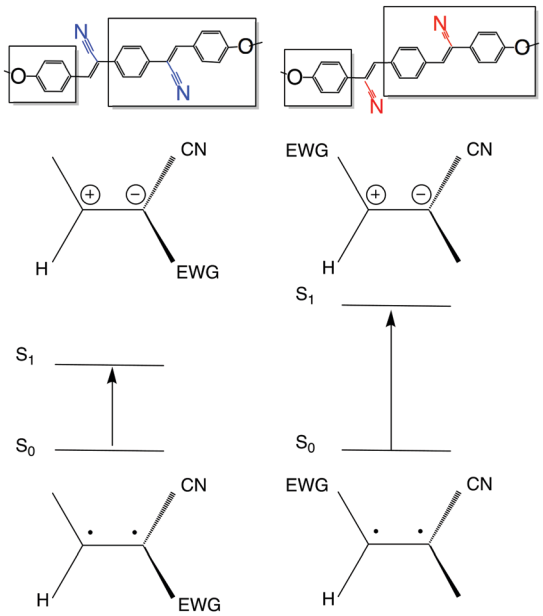

Fig. 12 Schematic representation of the zwitterionic structures of α,β-DMDCS at the pyramidalization region.

Fig. 12 shows a scheme of the excited state electronic structures for α,β-DMDCS derived from a CASSCF(12,12) wavefunction analysis, in which the two isomers are considered as functionalized ethene molecules. Four substituents can be distinguished; these are a hydrogen atom, a cyano group, 1-ring fragment, and 2-ring fragment. S_1 corresponds to a zwitterionic structure with two electrons on the C atom directly connected to the cyano group. This configuration is further stabilized if the other substituent on the same C atom is a stronger electron withdrawing group (EWG) than the substituents at the other part of the vinyl bond (zwitterionic stabilization, ZS). The 2-ring fragment (with electron affinity (EA) of 2.18 and 2.23 eV for α and β, respectively) is a stronger EWG than the 1-ring fragment (with EA of 0.2 eV).¶ Thus, α-DMDCS is much more stabilized than β-DMDCS.

For α,β-TFDCS, the EA difference between the 1-ring and 2-ring fragments is relatively lower than that for α,β-DMDCS, and it is not large enough to produce an inversion of the S_1 energy profiles (see Fig. 10). The EA of the 1-ring fragment for α,β-TFDCS is 1.51 eV and that of the 2-ring fragment for α-TFDCS and β-TFDCS is 2.75 and 2.69 eV, respectively. The EWGs CF_3 in the 1-ring fragment significantly increases its electron withdrawing character. For β-TFDCS, the inductive properties of 1-ring fragment compete with those of the 2-ring fragment. Overall, while ERS explains the trends in the FC region, ZS explains the trends in the pyramidalization region.

3.2.5. Quantum chemistry descriptors of the radiationless efficiency and luminescence. As demonstrated in the previous subsections, the analysis of the FC and pyramidalization regions helps in the interpretation of the emissive/non-emissive character of the DSB derivatives. Hence, representative quantities

¶ The EA was computed at the B3LYP/6-311G*/PCM($CHCl_3$) level of theory.

Table 3 Energy descriptors in eV, E_{va}, and $\Delta E_{(pyr)}$, computed at the CASPT2(12,12) level, and the k_{nr} in ns^{-1} for DSB, α,β-DMDCS, and α,β-TFDCS

Molecule	E_{va}	$\Delta E_{(pyr)}$	k_{nr} [a]
DSB	3.16	1.79	0.75
α-DMDCS	3.26	0.86	250
β-DMDCS	2.92	1.35	0.39
α-TFDCS	3.44	1.59	25.1
β-TFDCS	3.23	1.06	85.1

[a] Ref. 35.

at these regions can be chosen as descriptors for the luminescence. E_{va} is one of these descriptors which, as shown here and elsewhere,[35] correlates fairly well with the measured fluorescence quantum yields. The energy gap between S_1 and S_0 at the pyramidalization region is the other descriptor, hereafter, $\Delta E_{(pyr)}$. $\Delta E_{(pyr)}$ can be defined, for instance, at $\tau = 120^\circ$. Note that at the torsion region – before the C pyramidalization takes place – the energy gap is not able to predict the luminescence properties of the DCS molecules (see the CASPT2(12,12) energy profiles in the torsion region for α,β-DMDCS and α,β-TFDCS in Fig. 7 and 10, respectively).

Table 3 compiles the E_{va} and $\Delta E_{(pyr)}$ values for DSB, α,β-DMDCS, and α,β-TFDCS, together with the corresponding k_{nr} values.[35] For this series, E_{va} or $\Delta E_{(pyr)}$, as single independent variables do not correlate with $\log_{10} k_{nr}$. If E_{va} is the independent variable, the following regression model is obtained: $\log_{10} k_{nr} = 4.55E_{va} - 13.54$, where the coefficient of determination, R^2, is 0.47. If $\Delta E_{(pyr)}$ is the independent variable, the regression model is $\log_{10} k_{nr} = -2.35\Delta E_{(pyr)} + 4.17$, with R^2 of 0.51.‖ Conversely, a multiple regression with E_{va} and $\Delta E_{(pyr)}$, as independent variables, and $\log_{10} k_{nr}$ shows a better fitting. In this case, the regression model is $\log_{10} k_{nr} = 4.59E_{va} - 2.37\Delta E_{(pyr)} - 10.5$ with R^2 of 0.99.** These trends are preserved in general along the pyramidalization region.††

Based on the obtained correltations, $\Delta E_{(pyr)}$ is proposed to be the explanatory variable that improve the correlation between the computed E_{va} and experimental values. E_{va} and $\Delta E_{(pyr)}$ are relatively cheap descriptors for radiationless decays, thus, they may be used for systems where MECI determinations and photochemical reaction paths are computationally expensive or not affordable. Note that other descriptors have been proposed in the literature, such as the difference between the energy of the MECI and E_{va}, in relatively large molecules but at the SF-TDDFT level.[20] Our descriptors are entirely derived from CASSCF/CASPT2 wavefunctions and energies, which make them applicable to extended π-conjugated systems with many degenerate electronic configurations.

‖ A logarithmic regression model is chosen since the corresponding processes are expected to follow an activated Arrhenius-like behaviour. A linear regression model would lead to the same conclusions. In fact: $k_{nr} = 159.88E_{va} - 439.65$ ($R^2 = 0.08$), $k_{nr} = -233\Delta E_{(pyr)} + 382.15$ ($R^2 = 0.70$).

** A linear regression model between k_{nr} and E_{va} together with $\Delta E_{(pyr)}$ leads to: $k_{nr} = 163.33E_{va} - 233.59\Delta E_{(pyr)} - 140.03$ ($R^2 = 0.79$).

†† For instance, at $\tau = 150^\circ$, the regression model is: $\log_{10} k_{nr} = 4.22E_{va} - 2.72\Delta E_{(pyr)} - 7.36$ ($R^2 = 0.96$).

4. Conclusions

Through TDDFT and CASPT2 calculations, we have studied the non-radiative decay phenomenon in a representative group of cyano-substituted distyrylbenzene (DCS) molecules. Our conclusions are based on an approximated computational strategy to explore the S_0 and S_1 PESs avoiding computationally demanding and practically unfeasible photochemical reaction-path determinations and maintaining a full configuration interaction of the chemically-active orbitals and electrons. From the results obtained by applying the designed computational strategy, we have defined two simple energy descriptors for the prediction of non-radiative channels. These are the absorption energy, E_{va}, and the energy difference between S_0 and S_1 in the vicinity of the CI region, $\Delta E_{(pyr)}$. E_{va} and $\Delta E_{(pyr)}$ turned out to be qualitatively good to predict and explain the photophysical properties of the DCS compounds. While it is true that our strategy to explore the S_0 and S_1 PESs together with the descriptors are approximated, the latter correlate fairly well with the radiationless decay rates (k_{nr}). Larger k_{nr} values have been found for higher E_{va} coupled with lower $\Delta E_{(pyr)}$, as is the case for distyrylbenzene (DSB) and the β-isomer of the *para*-dimethoxy substituted DCS (β-DMDCS) molecule and the α-isomer of the *meta*-tetrafluoromethyl DCS (α-TFDCS) compound. On the contrary, α-DMDCS and β-TFDCS, with relatively higher emissive character (and low k_{nr}), have low E_{va} coupled with high $\Delta E_{(pyr)}$. We believe that our strategy is feasible and promising. Certainly, analogous strategies may be applied to other materials to predict the luminescence behavior.

Conflicts of interest

There are no conflicts to declare.

Acknowledgements

This publication is part of a European Joint Doctorate (EJD) in Theoretical Chemistry and Computational Modelling (TCCM), which has been financed under the framework of the Innovative Training Networks (ITN) of the MARIE Sklodowska-CURIE Actions (ITN-EJD-642294-TCCM). This work has been partially granted by the Ministerio de Economía y Competitividad (MINECO) through the project numbers CTQ2017-87054-C2-1-P and CTQ2017-87054-C2-2-P. The work performed in València has been partially supported by the Centers of Excellence in R&D program of the MINECO (MDM-2015-0538). The work performed in Madrid has been partially supported by Centers of Excellence in R&D program of the MINECO (SEV-2016-0686) and by the Campus of International Excellence (CEI) UAM + CSIC. The work performed in Seoul has been partially supported by the Creative Research Initiative Program through the National Research Foundation of Korea (NRF) funded by the Ministry of Science, ICT & Future Planning (MSIP; Grant No. 2009-0081571RIAM0417-20150013) and by Basic Science Research Program through the NRF funded by the Ministry of Science, ICT and Future Planning (Grant No. 2017R1E1A1A01075372).

M. A. I. acknowledges Vicente Pérez, from the Universitat de València, for his technical support on the use of the QCEXVAL facilities. D. R.-S. acknowledges the Ramón y Cajal grant (RYC-2015-19234) of the MINECO.

References

1 H. Dong, X. Fu, J. Liu, Z. Wang and W. Hu, *Adv. Mater.*, 2013, **25**, 6158–6183.
2 O. Ostroverkhova, *Handbook of organic materials for optical and (opto) electronic devices: properties and applications*, Elsevier, 2013.
3 Y. Li, *Organic optoelectronic materials*, Springer, 2015, vol. 91.
4 H. Usta, A. Facchetti and T. J. Marks, *Acc. Chem. Res.*, 2011, **44**, 501–510.
5 D. Oelkrug, A. Tompert, H.-J. Egelhaaf, M. Hanack, E. Steinhuber, M. Hohloch, H. Meier and U. Stalmach, *Synth. Met.*, 1996, **83**, 231–237.
6 K. H. Schweikart, M. Hohloch, E. Steinhuber, M. Hanack, L. Lüer, J. Gierschner, H.-J. Egelhaaf and D. Oelkrug, *Synth. Met.*, 2001, **1**, 1641–1642.
7 D. Oelkrug, A. Tompert, J. Gierschner, H.-J. Egelhaaf, M. Hanack, M. Hohloch and E. Steinhuber, *J. Phys. Chem. B*, 1998, **102**, 1902–1907.
8 J. Gierschner, M. Ehni, H.-J. Egelhaaf, B. Milián Medina, D. Beljonne, H. Benmansour and G. C. Bazan, *J. Chem. Phys.*, 2005, **123**, 144914.
9 J. Gierschner, J. Cornil and H. Egelhaaf, *Adv. Mater.*, 2007, **19**, 173–191.
10 B.-K. An, J. Gierschner and S. Y. Park, *Acc. Chem. Res.*, 2011, **45**, 544–554.
11 J. Gierschner and S. Y. Park, *J. Mater. Chem. C*, 2013, **1**, 5818–5832.
12 J. Gierschner, L. Lüer, B. Milián-Medina, D. Oelkrug and H.-J. Egelhaaf, *J. Phys. Chem. Lett.*, 2013, **4**, 2686–2697.
13 J. Shi, L. E. Aguilar Suarez, S.-J. Yoon, S. Varghese, C. Serpa, S. Y. Park, L. Lüer, D. Roca-Sanjuán, B. Milián-Medina and J. Gierschner, *J. Phys. Chem. C*, 2017, **121**, 23166–23183.
14 J. B. Birks, *Organic molecular photophysics*, Wiley, 1973.
15 A. W. Kohn, Z. Lin and T. Van Voorhis, *J. Phys. Chem. C*, 2019, **123**, 15394–15402.
16 L. Blancafort, R. Crespo-Otero and Q. Li, *Chem. – Asian J.*, 2019, DOI: 10.1002/asia.201801649.
17 M. G. S. Londesborough, J. Dolanský, L. Cerdan, K. Lang, T. Jelínek, J. M. Oliva, D. Hnyk, D. Roca-Sanjuán, A. Francés-Monerris and J. Martinčík, *Adv. Opt. Mater.*, 2017, **5**, 1600694.
18 M. A. Robb, *Conical Intersections: Theory, Computation and Experiment*, World Scientific, 2011, pp. 3–50.
19 K. Andersson, P. A. Malmqvist, B. O. Roos, A. J. Sadlej and K. Wolinski, *J. Phys. Chem.*, 1990, **94**, 5483–5488.
20 Y. Harabuchi, T. Taketsugu and S. Maeda, *Phys. Chem. Chem. Phys.*, 2015, **17**, 22561–22565.
21 X.-L. Peng, S. Ruiz-Barragan, Z.-S. Li, Q.-S. Li and L. Blancafort, *J. Mater. Chem. C*, 2016, **4**, 2802–2810.
22 Y.-J. Gao, X.-P. Chang, X.-Y. Liu, Q.-S. Li, G. Cui and W. Thiel, *J. Phys. Chem. A*, 2017, **121**, 2572–2579.
23 A. Prlj, N. Došlić and C. Corminboeuf, *Phys. Chem. Chem. Phys.*, 2016, **18**, 11606–11609.
24 X. Gao, Q. Peng, Y. Niu, D. Wang and Z. Shuai, *Phys. Chem. Chem. Phys.*, 2012, **14**, 14207–14216.
25 L. A. Estrada, A. Francés-Monerris, I. Schapiro, M. Olivucci and D. Roca-Sanjuán, *Phys. Chem. Chem. Phys.*, 2016, **18**, 32786–32795.
26 A. M. El-Zohry, D. Roca-Sanjuan and B. Zietz, *J. Phys. Chem. C*, 2015, **119**, 2249–2259.
27 M. G. S. Londesborough, J. Dolanský, T. Jelínek, J. D. Kennedy, I. Císařová, R. D. Kennedy, D. Roca-Sanjuán, A. Francés-Monerris, K. Lang and W. Clegg, *Dalton Trans.*, 2018, **47**, 1709–1725.
28 K. Andersson, P. Malmqvist and B. O. Roos, *J. Chem. Phys.*, 1992, **96**, 1218–1226.
29 D. Roca-Sanjuán, F. Aquilante and R. Lindh, *Wiley Interdiscip. Rev.: Comput. Mol. Sci.*, 2012, **2**, 585–603.
30 M. Barbatti, J. Paier and H. Lischka, *J. Chem. Phys.*, 2004, **121**, 11614–11624.
31 V. Molina, M. Merchán, B. O. Roos and P.-Å. Malmqvist, *Phys. Chem. Chem. Phys.*, 2000, **2**, 2211–2217.
32 Y. Amatatsu, *J. Comput. Chem.*, 2002, **23**, 950–956.
33 I. N. Ioffe and A. A. Granovsky, *J. Chem. Theory Comput.*, 2013, **9**, 4973–4990.
34 D. H. Waldeck, *Chem. Rev.*, 1991, **91**, 415–436.
35 J. Shi, M. A. Izquierdo, S. Oh, S. Y. Park, B. Milián-Medina, D. Roca-Sanjuán and J. Gierschner, *Org. Chem. Front.*, 2019, **6**, 1948–1954.
36 N. Minezawa and M. S. Gordon, *J. Phys. Chem. A*, 2011, **115**, 7901–7911.
37 T. Yanai, D. P. Tew and N. C. Handy, *Chem. Phys. Lett.*, 2004, **393**, 51–57.
38 M. J. Frisch, G. W. Trucks, H. B. Schlegel, G. E. Scuseria, M. A. Robb, J. R. Cheeseman, G. Scalmani, V. Barone, B. Mennucci and G. A. Petersson, *Gaussian 09, revision A.1*, Gaussian Inc., Wallingford, CT, 2009, **27**, 34.
39 R. A. Kendall, T. H. Dunning Jr and R. J. Harrison, *J. Chem. Phys.*, 1992, **96**, 6796–6806.
40 F. Aquilante, J. Autschbach, R. K. Carlson, L. F. Chibotaru, M. G. Delcey, L. De Vico, I. Fdez. Galván, N. Ferré, L. M. Frutos and L. Gagliardi, *J. Comput. Chem.*, 2016, **37**, 506–541.
41 K. Pierloot, B. Dumez, P.-O. Widmark and B. O. Roos, *Theor. Chim. Acta*, 1995, **90**, 87–114.
42 M. Cossi, V. Barone, R. Cammi and J. Tomasi, *Chem. Phys. Lett.*, 1996, **255**, 327–335.
43 N. Forsberg and P.-Å. Malmqvist, *Chem. Phys. Lett.*, 1997, **274**, 196–204.
44 G. Ghigo, B. O. Roos and P. Å. Malmqvist, *Chem. Phys. Lett.*, 2004, **396**, 142–149.
45 B. G. Levine and T. J. Martínez, *Annu. Rev. Phys. Chem.*, 2007, **58**, 613–634.
46 M. Ben-Nun and T. J. Martínez, *Chem. Phys. Lett.*, 1998, **298**, 57–65.

47 D. A. Condirston and J. D. Laposa, *Chem. Phys. Lett.*, 1979, **63**, 313–317.
48 J. L. Charlton and J. Saltiel, *J. Phys. Chem.*, 1977, **81**, 1940–1944.
49 M. E. Mortenson, *Mathematics for computer graphics applications*, Industrial Press Inc., 1999.
50 S. Varghese, S. K. Park, S. Casado, R. C. Fischer, R. Resel, B. Milián-Medina, R. Wannemacher, S. Y. Park and J. Gierschner, *J. Phys. Chem. Lett.*, 2013, **4**, 1597–1602.
51 K. Sandros, M. Sundahl, O. Wennerstroem and U. Norinder, *J. Am. Chem. Soc.*, 1990, **112**, 3082–3086.
52 M. Sundahl, O. Wennerstroem, K. Sandros, T. Arai and K. Tokumaru, *J. Phys. Chem.*, 1990, **94**, 6731–6734.
53 A. Nenov and R. de Vivie-Riedle, *J. Chem. Phys.*, 2012, **137**, 74101.
54 J. González-Vázquez and L. González, *Chem. Phys.*, 2008, **349**, 287–295.